A visibility-based approach using regularization for imaging-spectroscopy in solar X-ray astronomy

2008 J. Phys.: Conf. Ser. 135 012084

(http://iopscience.iop.org/1742-6596/135/1/012084)

Journal of Physics: Conference Series **135** (2008) 012084 doi:10.1088/1742-6596/135/1/012084

A visibility-based approach using regularization for imaging-spectroscopy in solar X-ray astronomy

M Prato[1], A M Massone[1], M Piana[1,2], A G Emslie[3], G J Hurford[4], E P Kontar[5] and R A Schwartz[6]

[1] CNR - INFM LAMIA, Via Dodecaneso 33 I-16146 Genova, Italy
[2] Dipartimento di Informatica, Università di Verona, Ca' Vignal 2, Strada le Grazie 15, I-37134 Verona, Italy
[3] Department of Physics, Oklahoma State University, Stillwater, OK 74078
[4] Space Sciences Laboratory, University of California at Berkeley, 8 Gauss Way, Berkeley, CA 94720-7450
[5] Department of Physics & Astronomy, The University, Glasgow G12 8QQ, Scotland, UK
[6] CUA (Catholic University) and LSSP at NASA Goddard Space Flight Center, code 671.1 Greenbelt, MD 20771

E-mail: massone@ge.infm.it

Abstract. The Reuven Ramaty High-Energy Solar Spectroscopic Imager (RHESSI) is a nine-collimators satellite detecting X-rays and γ-rays emitted by the Sun during flares. As the spacecraft rotates, imaging information is encoded as rapid time-variations of the detected flux. We recently proposed a method for the construction of electron flux maps at different electron energies from sets of count visibilities (i.e., direct, calibrated measurements of specific Fourier components of the source spatial structure) measured by RHESSI. The method requires the application of regularized inversion for the synthesis of electron visibility spectra and of imaging techniques for the reconstruction of two-dimensional electron flux maps. The method, already tested on real events registered by RHESSI, is validated in this paper by means of simulated realistic data.

1. Introduction

There exist important astronomical techniques in which the observed temporal modulation is interpreted in terms of *visibilities* [1], which are calibrated measurements of specific spatial Fourier components of the radiation emitted by the remote source. This happens, for example, in radio interferometry [2] but also in X-ray imaging, when the instrument employs a Rotating Modulation Collimator (RMC) imaging technique [3], in which rapid time variations of the detected counts are induced by the presence of a grid with a specific pitch in front of the detector. For these imaging modalities, visibilities represent the purest possible measurements: they are fully calibrated since they contain no instrument dependence other than spatial frequencies; their statistical error is well defined since they are linear combinations of binned counts; owing to symmetry properties of the imaging system, they offer redundant information, thus providing indication of systematic errors; finally, visibilities depend linearly on the source flux, and therefore visibilities of a multi-component source can be considered as the sum of the visibilities of its components, thus facilitating the measurements' interpretation.

Making imaging with visibilities is relatively easy, since they provide the input data for Fourier-based reconstruction methods which reduce the artifacts due to incomplete components by means of some regularization procedure. However, most radioastronomical and RMC imaging techniques are designed in order to provide images of the source at different radiation energies in an imaging spectroscopy framework, and deducing reliable spectral properties from images at different energies is not an easy task. A very natural procedure (and this is indeed the traditional approach to imaging spectroscopy) consists of the following steps [4]:

- A Fourier-based image reconstruction technique is applied to each visibility set, for each energy. This leads to a set of reconstructed images of the source radiation at different energy channels.
- Physically significant clusters of pixels are pointed out and corresponding spectra are constructed by means of a simple re-ordering procedure, i.e. the pixel contents for the same specific cluster at different energies are summed up to produce a two-dimensional profile of the radiation flux of the cluster as a function of the radiation energy (or wavelength).

This scheme has two very significant drawbacks. First, the images reconstructed from visibilities are strongly uncorrelated in energy since no regularization is performed in the spectral direction (the image reconstruction method provides only spatial smoothing) and this is not realistic, since it is physically sound to assume that images of the same source corresponding to adjacent energy channels have similar spatial properties. Second, astronomical observations are typical remote sensing procedures, where the reconstructed radiation flux images in general provide very indirect information on source parameters of real physical interest (properties of the plasma like temperature distribution or electron flux are much more instructive, from a physical perspective, than reconstructions of the spatial distribution of the radiation flux). From a mathematical viewpoint, the relation between the radiation flux spectrum and the parameter of interest at different energies is often modeled by an integral equation whose smearing kernel provides an indication of the loss of information consequence of the physical process occuring in the source site.

A solution to these drawbacks is a modification of the previous approach, whereby the radiation flux spectrum obtained at the end of the second step is inverted (regularizing this time in the energy direction) to obtain a smoothed parameter profile as a function of the parameter energy (parameter spectrum) and then images of the parameter at different energies are obtained through pixel reordering. However this solution is not satisfactory for two reasons. First, it is computationally heavy: in order that such an approach works, the inversion should be done for very small clusters (even for all spectra corresponding to one pixel) thus requiring a notable amount of regularization procedures. Second, spectral inversion is typically a very ill-posed problem and if the input data are not reliable spurious components may not be eliminated even if regularization is applied: in this approach the input data are the pixel contents of the reconstructed images which, due to the reconstruction procedure adopted, will be significantly different than the emitted flux.

In the present paper we describe and validate a different approach to imaging spectroscopy with visibilities [5]. This approach is based on the following observation: both Fourier transform and the integral transformation relating the radiation flux spectrum and the parameter spectrum are linear. Therefore, for the same spatial frequencies sampled by the count visibilities and at different energies, it makes sense to define sets of auxiliary visibilities associated with the unknown parameters of physical interest. Then imaging spectroscopy can be performed in the following way:

- For each spatial frequency a re-ordering procedure allows one to construct a count visibility spectrum. This spectrum is related to the visibility spectrum associated to the

unknown parameter for the same spatial frequency by means of the same ill-posed integral transformation relating the count and the parameter spectra.

- Each count visibility spectrum is inverted to obtain a regularized visibility spectrum for the unknown parameter.
- A new re-ordering procedure and the application of a Fourier-based image reconstruction algorithm allows one to obtain two-dimensional maps of the source parameter at different energies.

This new approach presents some clear advantages: the parameter maps are more significant than the count maps from a physical viewpoint; furthermore, thanks to spectral regularized inversion, a smoothing constraint in the energy direction is inserted; finally, from a computational viewpoint, these maps can be obtained by inverting a relatively small number of visibility count spectra.

The plan of the paper is as follows. In Section 2 the reconstruction algorithm is described in the setting provided by the solar X-ray satellite Reuven Ramaty High Energy Solar Spectroscopic Imager (RHESSI) [6]. In Section 3 a validation of the method is performed for sets of synthetic visibilities. Our conclusions are offered in Section 4.

2. Imaging spectroscopy for RHESSI

The idea at the basis of the RHESSI imaging technique is to modulate the X-ray emission during solar flares [7]. RHESSI utilizes nine rotating collimators with grids of different pitch in order to modulate the solar radiation and nine germanium detectors to measure the energy of each incident photon very precisely. Thanks to its hardware RHESSI is able to perform hard X-ray imaging at an angular resolution in the range $2-7$ arcseconds, a temporal resolution of tens of milliseconds, in the energy range from 3 keV to 400 keV; and hard X-ray spectroscopy with a spectral resolution from 0.5 keV to 2 keV, in the same energy range. In RHESSI, spatial information is encoded in the temporal modulation of the detected flux: as the collimator rotates, the amplitude and phase of this pseudoperiodic modulation over a limited range of angles provides a direct, calibrated measurement of a single Fourier component of the source distribution. The spatial frequency of this measured visibility is determined by the angular resolution of the collimator and its instantaneous orientation. Combining data from multiple rotating collimators at a variety of orientations, the set of visibilities can then be used to reconstruct the spatial distribution of the source. Since visibilities can be summed linearly, this perspective on the data provides a convenient basis for combining data from multiple rotations into a tractable number of visibility measurements with well-defined statistical errors.

A simplified description of this imaging approach is as follows. For each time point of a modulation profile a roll angle can be defined and binned into several (twelve in the case of RHESSI) aspect phases measuring the position of the source with respect to some reference point in the collimator grid. Owing to the angular drift of the satellite axis, for different rotations, different phases correspond to the same roll angle. In order to increase the signal-to-noise ratio, roll angles and aspect phases are accumulated into roll and phase bins and the corresponding counts are stacked into nine histograms, one for each collimator. The last step for the visibility construction is to fit by a Fourier series the count profile in the histogram as a function of the phase bin. The visibility is therefore a complex number whose real and imaginary parts are proportional to the first two coefficients of the fitting Fourier series. It follows that, roughly speaking, a visibility at a specific count energy is a complex number representing the Fourier transform of the count flux at a particular point in the frequency plane. Because of the rotating modulation collimator design of RHESSI, these visibilities are sampled on cylindrical profiles with radii equal to the inverse spatial period of the imaging grids (figure 1).

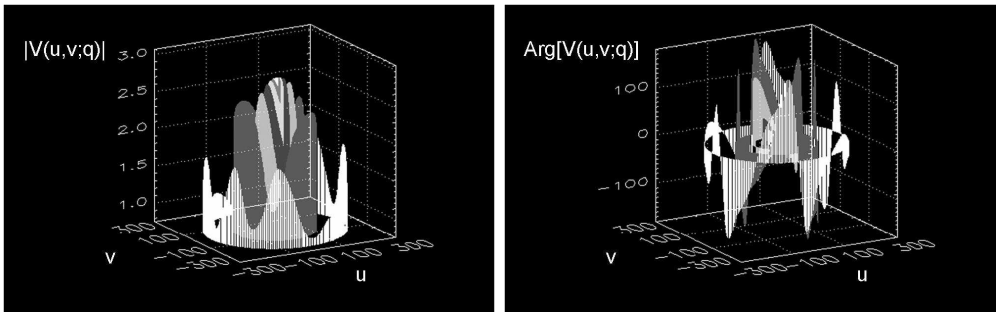

Figure 1. Visibility amplitude (*left panel*) and phase (*right panel*). Visibilities are sampled at discrete points along circular tracks at specific spatial frequencies whose magnitude is the inverse of the angular resolution of each collimator.

The starting point for our approach is the following formal definition of visibility based on the previous discussion. For each one of the nine RHESSI detectors, the visibility (counts cm^{-2} s^{-1} keV^{-1}) at spatial frequency (u, v) and count energy q is given by

$$V(u,v;q)dq = \int_x \int_y \int_{\epsilon=q}^{\infty} D(q,\epsilon) I(x,y;\epsilon) e^{2\pi i(ux+vy)} d\epsilon dx dy \quad , \tag{1}$$

where $I(x, y; \epsilon)$ (photons cm^{-2} s^{-1} keV^{-1} arcsec^{-2}) is the value of the photon flux of energy ϵ at point (x, y) of the imaging plane; $D(q, \epsilon)$ is the differential element of the Detector Response Matrix[1] (DRM) corresponding to the generation of a count with energy in the energy range $[q, q + dq]$ from a photon in the energy range $[\epsilon, \epsilon + d\epsilon]$.

It is well established [8] that the physical process which relates hard X–ray emission to electron acceleration in the plasma is essentially collisional Bremsstrahlung. Then, if we introduce the mean source electron flux at point (x, y), $\overline{F}(x, y; E)$ (electrons cm^{-2} s^{-1} keV^{-1}), responsible for the $I(x, y; \epsilon)$ emission, in this imaging spectroscopy framework, such process is described by the Volterra integral equation of the first kind

$$I(x,y;\epsilon) = \frac{a^2}{4\pi R^2} \int_{\epsilon}^{\infty} N(x,y) \overline{F}(x,y;E) Q(\epsilon,E) dE \quad . \tag{2}$$

Here $N(x, y)$ is the column density (cm^{-2}) at each point (x, y) in the image, $a = 7.25 \times 10^7$ cm arcsec^{-2}, $R = 1$ AU and $Q(\epsilon, E)$ is the Bremsstrahlung cross-section (cm^2 keV^{-1}) which we will assume according to formula 3BN in the Koch and Motz paper [9], i.e., isotropic, fully relativistic with Coulomb correction at small energies.

Inspired by the count visibility spectrum defined by equation (1), for each electron energy E we introduce the auxiliary electron visibilities (electrons cm^{-2} s^{-1} keV^{-1})

$$W(u,v;E) = a^2 \int_x \int_y N(x,y) \overline{F}(x,y;E) e^{2\pi i(ux+vy)} dx dy \quad . \tag{3}$$

A very simple computation exploiting the linearity of all the relations introduced so far, leads from equations (1)–(3) to

$$V(u,v;q) = \frac{1}{4\pi R^2} \int_q^{\infty} W(u,v;E) K(q,E) dE \quad , \tag{4}$$

[1] The DRM is a structured matrix accounting for many detector properties like the attenuator and blanket transmission, the response to modulated photons and the detector resolution.

Table 1. Algorithm for the synthesis of electron flux spectrum images

1 **For each detector and each frequency pair** (u, v) **for which visibilities are available:**

- *(a) construct a count visibility spectrum* $V(u, v; q)$*, i.e. count visibilities versus the corresponding count energies;*
- *(b) apply a regularized inversion to obtain an electron visibility spectrum* $W(u, v; E)$*, i.e. electron visibilities versus the corresponding electron energies.*

2 **For each detector and each electron energy:**

- *(a) construct the set of corresponding electron visibilities.*

3 **For each electron energy:**

- *(a) apply some Fourier-based image processing method to construct the electron flux map.*

where

$$K(q, E)dq = \int_q^\infty D(q, \epsilon)Q(\epsilon, E)d\epsilon \quad . \tag{5}$$

Equation (4) naturally inspires the algorithm summarized in table 1 for the synthesis of electron flux spectrum images. In some more details, step 1(a) and step 2(a) of the algorithm are essentially re-ordering procedures: in step 1(a) we fix a point in the frequency space and take all visibilities with different count energies corresponding to that point; in step 2(a) we fix the energy (and the detector) and take all visibilities with different frequencies corresponding to that electron energy. Regularized inversion in step 1(b) is performed by Tikhonov zero-order regularization [10]. This approach allows us to address equation (4) as a rectangular problem and therefore to reconstruct $W(u, v; E)$ up to electron energies significantly bigger than the count energies in the data. The image synthesis in the final step 3(a) is realized by applying a Maximum Entropy (MEM-NJIT) algorithm [11].

3. Validation of the method

In [5], the method described in the previous section has been presented and tested on real data with results physically consistent. Here we give a validation of the method by testing it on simulated but realistic images. The simulations are performed according to the following steps:

- we build the theoretical mean source electron flux images for each electron energy channel (i.e. $\overline{F}(x, y; E)$);
- for a fixed count energy q (i.e., for a fixed count map) we compute the count flux emitted from each position (x, y) through the Bremsstrahlung equation (2) and taking into account the DRM contribution. The iteration of this procedure for each count energy channel leads to a set of theoretical count maps produced by the theoretical electron maps simulated in the previous step;
- for each energy channel, we apply the Fourier transform to the count maps (equation 1) to obtain the count visibilities at different spatial frequencies. This set of count visibilities is completely equivalent to the visibilities measured by RHESSI. In a similar way it is possible to compute the theoretical electron visibilities by applying the Fourier transform to the simulated mean source electron flux maps. We also affect these count visibilities with noise which accounts for both count statistics and some systematic error typical of RHESSI detectors.

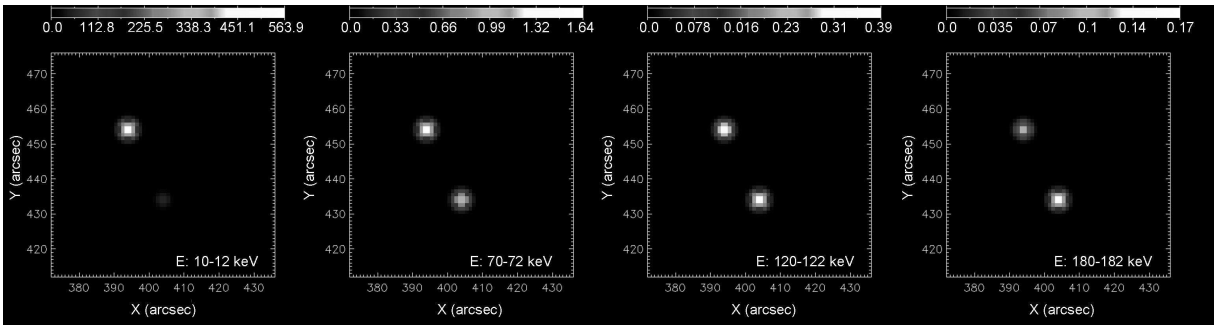

Figure 2. *From left to right:* Simulated electron maps corresponding to the energy channels 10-12 keV, 70-72 keV, 120-122 keV and 180-182 keV.

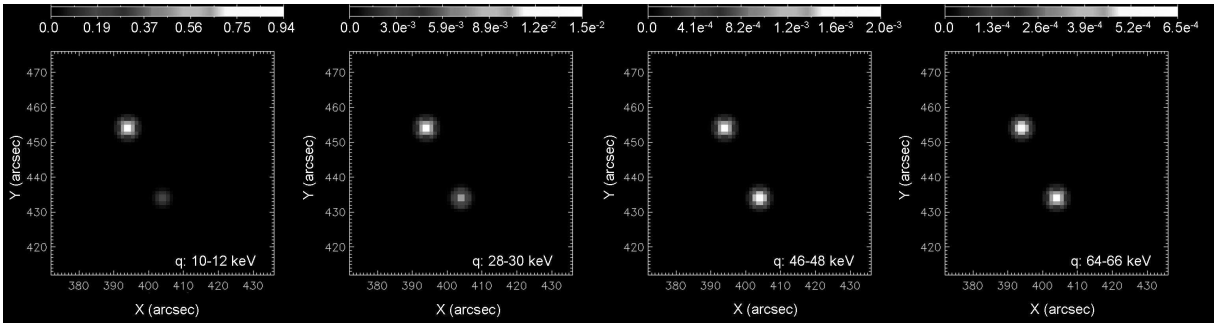

Figure 3. *From left to right:* Computed count maps corresponding to the energy channels 10-12 keV, 28-30 keV, 46-48 keV and 64-66 keV.

The application of our inversion algorithm to the set of theoretical count visibilities provides an excellent test for the validation of the method because after the inversion we are able to compare the electron maps resulting from the regularized electron visibilities to the original simulated ones. Here we present the results we obtained when an event characterized by two footpoints is simulated. The flux intensity of each footpoint has been simulated as a Gaussian function, centered in the point (x_j, y_j) (where $j = 1, 2$) of the image, whose standard deviation σ_j describes the smearing around the center. Each Gaussian is then modulated along the energy direction by a single power-law with spectral index δ_j:

$$\overline{F}(x, y; E) = A_1 E^{-\delta_1} e^{-\frac{\|(x,y)-(x_1,y_1)\|_2^2}{2{\sigma_1}^2}} + A_2 E^{-\delta_2} e^{-\frac{\|(x,y)-(x_2,y_2)\|_2^2}{2{\sigma_2}^2}} . \qquad (6)$$

For the first source we set (x_1, y_1)=(394 arcsec, 454 arcsec), $\sigma_1 = 1.6$ and $\delta_1 = 3$. The second source, located at (404 arcsec, 434 arcsec), is less bright than the first one for the first energy channel but its brightness decreases more slowly as the energy increases ($\delta_2 = 2$). The width of the source is the same as before ($\sigma_2 = 1.6$). We simulated 95 electron maps from 10 keV up to 200 keV with a step of 2 keV and we built the corresponding count maps from 10 keV to 100 keV (again with a step of 2 keV) by using the Bremsstrahlung equation as previously described. In figures 2 and 3 some of these simulated electron and count maps are shown.

We sampled 224 (u, v) pairs in the u, v-plane, as previously described, and we computed the corresponding visibility values by Fourier transforming both the count and the electron maps. Figure 4 shows the real and imaginary parts respectively for a count visibility spectrum

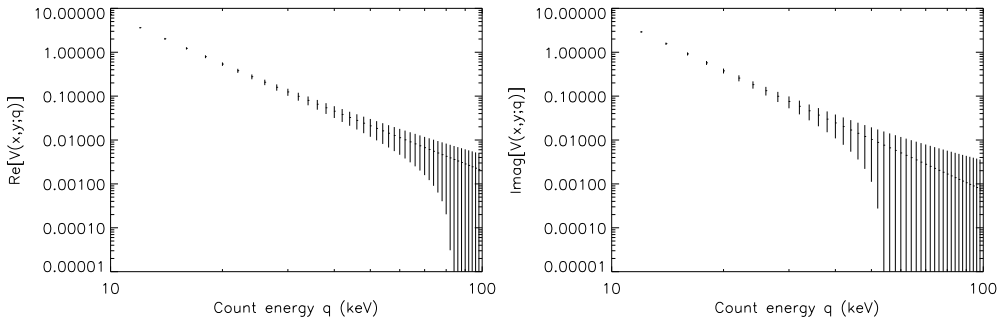

Figure 4. Real part (*left panel*) and imaginary part (*right panel*) (counts cm^{-2} s^{-1} keV^{-1}) of the count visibility spectrum V(u^*, v^*; q) at the point (u^*, v^*).

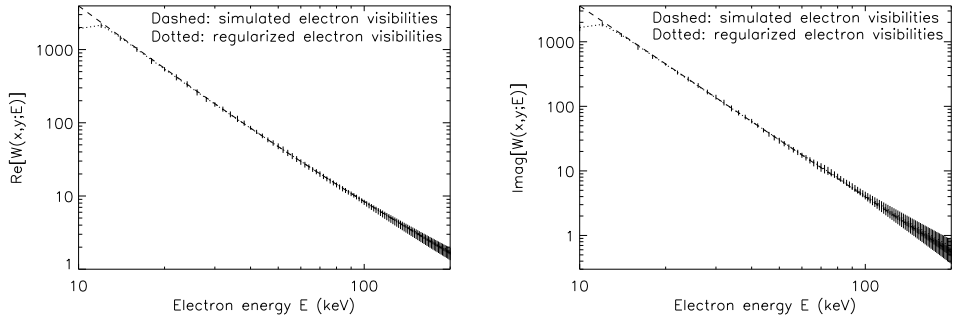

Figure 5. Real part (*left panel*) and imaginary part (*right panel*) (electrons cm^{-2} s^{-1} keV^{-1}) of the electron visibility spectrum W(u^*, v^*; E) at the point (u^*, v^*).

V(u^*,v^*;q) corresponding to a fixed (u^*,v^*) frequency pair while in figure 5 the regularized electron visibility spectra resulting from the inversion procedure (dotted lines) are successfully compared to the theoretical ones (dashed lines). For each electron energy it is now possible to construct the set of corresponding visibilities and to apply the MEM-NJIT algorithm for the synthesis of electron flux images. Visually, the reconstructed electron maps (figure 6) are comparable to the simulated ones (figure 2) but a more quantitative comparison is given in figure 7 where starting from reconstructed electron images, electron flux spectra extracted from small regions around the two footpoints or from the whole image are superimposed to the theoretical ones. In the first plot the local fluxes are slightly underestimated as a consequence of the smearing of the sources with respect to the original ones. Moreover, in the second plot, the accordance between simulated and reconstructed total flux is clearly evident.

4. Comments

We presented a validation of a new approach to imaging spectroscopy in the case of RMC imaging techniques. The method is tested in the case of synthetic data produced according to the framework of the X-ray solar spectroscopic imager RHESSI. The method produces reliable regularized reconstructions of electron maps of a solar flare from which local and total electron flux spectra of physical interest can be extracted.

From a theoretical viewpoint two issues which should be investigated to improve the method

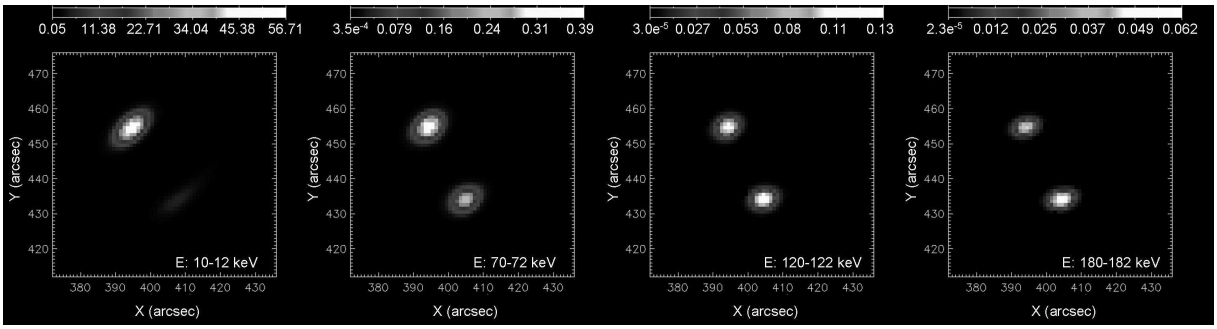

Figure 6. Regularized electron maps produced using the regularized electron visibilities and the MEM-NJIT algorithm. The energy channels are the same of figure 2.

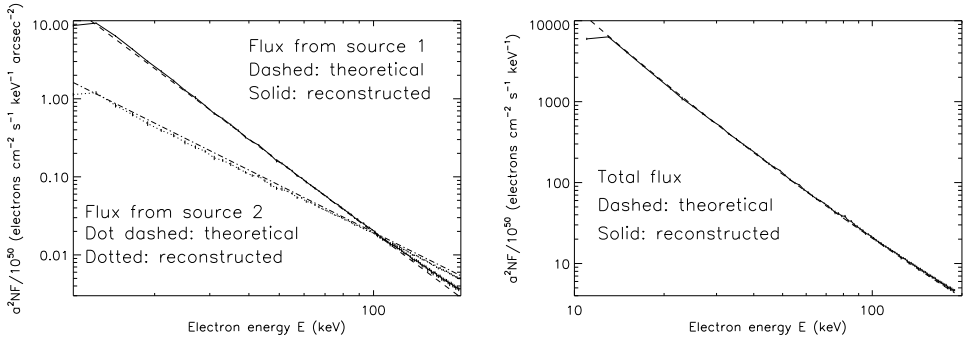

Figure 7. Local fluxes (*left panel*) and total flux (*right panel*) (electrons cm^{-2} s^{-1} keV^{-1} arcsec^{-2}) extracted from the theoretical and reconstructed electron images.

are concerned with the use of possibly more effective regularization techniques for both spectral inversion and, particularly, image reconstruction. More in general, we think that this approach can be rather easily generalized to any parametric imaging spectroscopy which utilizes visibilities as input data.

Acknowledgments
The Swiss International Space Science Institute (ISSI) is kindly acknowledged.

References
[1] Prince T A et al *Solar Phys.* **118** 269
[2] Thompson A R, Moran J M and Swenson G W 2001 *Interferometry and Synthesis in Radioastronomy* (Wiley)
[3] Smith D M, Hurford G J and Boggs S E 2004 *New Astronomy Rev.* **48** 209
[4] Emslie A G, Kontar E P, Krucker S and Lin R P 2003 *Astrophys. J.* **595** L107
[5] Piana M, Massone A M, Hurford G J, Prato M, Emslie A G, Kontar E P and Schwartz R A 2007 *Astrophys. J.* **665** 846
[6] Lin R P et al 2002 *Solar Phys.* **210** 3
[7] Hurford G J et al 2002 *Solar Phys.* **210**, 61
[8] Brown J C, Emslie A G and Kontar E P 2003 *Astrophys. J.* **595** L115
[9] Koch H W and Motz J W 1959 *Rev. Mod. Phys.* **31** 920
[10] Piana M, Massone A M, Kontar E P, Emslie A G, Brown J C and Schwartz R A 2003 *Astrophys. J.* **595** L123
[11] Bong S C, Lee J, Gary D E and Yun H S 2006 *Astrophys. J.* **636** 1159